



UNIVERSITY OF LEEDS

This is a repository copy of *Quantitative Impact of Fluid vs. Solid Interfaces on the Catalytic Performance of Pickering Emulsions*.

White Rose Research Online URL for this paper:
<https://eprints.whiterose.ac.uk/170197/>

Version: Accepted Version

Article:

Stock, S, Schlander, A, Kempin, M et al. (10 more authors) (2020) Quantitative Impact of Fluid vs. Solid Interfaces on the Catalytic Performance of Pickering Emulsions. *Physical Chemistry Chemical Physics*. ISSN 1463-9076

<https://doi.org/10.1039/d0cp06030e>

© the Owner Societies 2021. This is an author produced version of an article published in *Physical Chemistry Chemical Physics*. Uploaded in accordance with the publisher's self-archiving policy.

Reuse

Items deposited in White Rose Research Online are protected by copyright, with all rights reserved unless indicated otherwise. They may be downloaded and/or printed for private study, or other acts as permitted by national copyright laws. The publisher or other rights holders may allow further reproduction and re-use of the full text version. This is indicated by the licence information on the White Rose Research Online record for the item.

Takedown

If you consider content in White Rose Research Online to be in breach of UK law, please notify us by emailing eprints@whiterose.ac.uk including the URL of the record and the reason for the withdrawal request.



eprints@whiterose.ac.uk
<https://eprints.whiterose.ac.uk/>

Cite this: DOI: 00.0000/xxxxxxxxxx

Quantitative Impact of Fluid vs. Solid Interfaces on the Catalytic Performance of Pickering Emulsions[†]

Sebastian Stock,^a Annika Schlander,^b Maresa Kempin,^c Ramsia Geisler,^a Dmitrij Stehl,^a Kai Spanheimer,^a Nicole Hondow,^d Stuart Micklethwaite,^d Ariane Weber,^e Reinhard Schomäcker,^e Anja Drews,^c Markus Gallei,^b and Regine von Klitzing^{*a}

Received Date
Accepted Date

DOI: 00.0000/xxxxxxxxxx

Pickering emulsions (PEs) i. e. particle stabilized emulsions, are used as reaction environment in biphasic catalysis for the hydroformylation of 1-dodecene into tridecanal using the catalyst rhodium (Rh)-sulfoxantphos (SX). The present study connects knowledge about particle catalyst interaction and PE structure with reaction results. It quantifies the efficiency of the catalytic performance of the catalyst localized in the voids between the particles (liquid-liquid interface) and catalyst adsorbed on the particles surface (liquid solid interface) by a new numerical approach. First, it is demonstrated that the overall packing density and geometry at the droplet interface and the size of the water droplets of the resulting w/o PEs are predictable by a simple model as confirmed by cryogenic scanning electron microscopy (cryo-SEM) imaging. Second, it is shown that approximately all particles used for emulsification assemble at the droplet surface after emulsion preparation and neither the packing parameter nor the droplet size change with particle surface charge or size when the total particle cross section is kept constant. Third, studies on the influence of the catalyst on the emulsion structure reveal that ir respectively of the particles charge the surface active and negatively charged catalyst Rh-SX reduces the PEs droplet size significantly and decreases the particle packing parameter from $s = 0.91$ (hexagonal packing in 2D) to $s = 0.69$ (shattered structure). In this latter case, large voids of free w/o interface form and become covered with catalyst. With this deep knowledge about the PE structure the reaction efficiency of liquid-liquid vs. solid-liquid interfaces are quantified. By excluding any other influence factors, it is shown that the activity of the catalyst is the same at the fluid and solid interface and the performance of the reaction is explained by the geometry of the system. After the reaction, the product separation via membrane filtration is shown to be successfully applicable without damaging the emulsions. This enables almost complete recovery of the catalyst i. e. the most expensive compound in PE-based catalytic reactions, being a crucial criterion for industrial applications.

1 Introduction

Pickering emulsions (PEs) are emulsions stabilized by solid or soft particles^{1,2}. The understanding of their physico-chemical properties and their cost-effective and simple preparation procedure al-

lows for application in many fields of research. They are successfully used in medicine³, cosmetics⁴, food industry⁵ and material synthesis⁶. The PE's strong resistance against coalescence while increasing the interface between two immiscible liquids makes them excellent candidates as reaction environment for catalysis. The use of PEs is beneficial for various applications in the biphasic biocatalysis⁷⁻⁹ but also for many other biphasic reactions for example hydrogenation^{10,11}, olefin epoxidation^{12,13}, acetalization of aldehydes¹⁴, and other catalytic reactions¹⁵⁻¹⁸.

In this study, the influence of the PE structure on the catalysis and catalyst recovery is investigated on the basis of the hydroformylation of the long chained olefin 1-dodecene into the aldehyde

^a Department of Condensed Matter Physics, Technische Universität Darmstadt, Darmstadt, Germany.; Tel: +49-(0)6151-16-24506; E-mail: klitzing@smi.tu-darmstadt.de

^b Ernst Berl-Institute for Technical and Macromolecular Chemistry, Technische Universität Darmstadt, Darmstadt, Germany

^c Department II, Process Engineering in Life Science Engineering, HTW Berlin, Berlin, Germany

^d School of Chemical and Process Engineering, University of Leeds, Leeds, UK

^e Department of Technical Chemistry, Technische Universität Berlin, Berlin, Germany

tridecanal. This reaction is catalysed via the water soluble catalyst complex rhodium-sulfoxantphos (Rh-SX) in varied PE environment. As recovery method membrane filtration for the retention of catalyst containing water droplets is evaluated. Earlier studies on this system dealt with the general feasibility of the hydroformylation in PEs^{19–24}. In this context Stehl et al.²⁴ showed that a positive surface charge on the surface of Halloysite nanotubes is more beneficial for the product yield than a negative one. Zhao et al.²² and Tao et al.²³ used positively charged silica spheres and compared them to positively charged mesoporous silica spheres and speculated that the porosity facilitates mass transport through the particle layer. They found that the adsorption of the negatively charged catalyst onto the positively charged particles is beneficial for the reaction. Results from these earlier works imply that on the one hand the surface occupation by the particles provides the desired high stability, but on the other hand it hinders the interfacial contact between oil and water and therefore hinders the mass transfer.

Very fundamental studies for different particle systems for PEs in general were carried out by Binks et al.. The influence of size²⁵ and hydrophobicity is well understood for different nanoparticle systems. The hydrophobicity of the particles defines the ability of the particles to attach to the interface and dictates the resulting emulsion type^{26–28}. A model for the prediction of the droplet diameter after the initial fast coalescence process finished is called *limited coalescence model*. It was first proposed by R. M. Wiley in 1954²⁹ and was refined and proven for different systems^{30–33}. While a general understanding of the influence of various particle properties on PE properties was established, the transfer of this information to the catalytic reaction process in the PE environment stays speculative.

In consequence, an often underestimated challenge when comparing results by various authors for finding an adequate model system and also for developing analytical models for the desired catalytic process is the low comparability between different particle systems and the lack of quantitative parameters describing those. So far, the particles of different studies and also within the same study vary in a whole bunch of parameters. Therefore, the prediction and identification of dominant properties influencing the reaction behaviour is very difficult or even impossible and deducing conceptual conclusions becomes often speculative. Differences in particle shape, size and hydrophobicity may lead to a varied water/oil droplet size, may affect the fraction of particles being able to adsorb at the interface or may also affect the particles packing geometry and density at the droplet surface. Both, the droplet size and the packing condition, may influence the mass transfer and with that the reaction outcome such as yield and conversion rate. A deeper physico-chemical understanding of the system is needed for improving the catalytic performance in PEs beyond trial and error or fine tuning approaches. Therefore, for the exact prediction of reaction outcomes for future PE formulations it is essential to understand the effect of different particle properties as well as their interaction with the catalyst on the PE structure and subsequently on the reaction performance in detail. In summary, this article addresses the following questions: I) How exactly does the interaction between negatively charged

catalyst molecules and positively charged particles influence the catalyst substrate contact?; II) How does the presence of a surface active and particle adsorbing catalyst influence the PE structure?; III) How does the catalysts physico-chemical properties of the catalyst influence the reaction and filtration process?; and finally IV) Is the void area between the particles or the particle surface area pointing into the oil phase important for the efficiency? - a fundamental question for the emulsion design. In order to answer these questions without leaving open alternative explanations for the observed effects (particle properties, droplet size etc.) the present study is conducted in a bottom up approach. First, silica nanospheres are synthesized that differ only in one feature: either charge or size. Second, the effect of the tailored particle properties and catalyst on the resulting PEs structure is determined. Third, the impact of several parameters on the reaction are considered. The w/o emulsion type is used because it allows to retain the water soluble catalyst in the water droplets while separating the product phase. Finally, the surface coverage and its impact on the reaction results are determined and discussed in detail. This includes the discussion on the effect of particle size and particle surface charge. In addition to this and in order to find further explanations for the earlier found increase in reaction performance for positively charged particles the particle/catalyst interaction was investigated. In view of the envisaged continuous PE reaction process, the influence of particle properties on membrane filtration is finally studied.

2 Experimental Section

2.1 Material

Water with $\rho = 18.2 \text{ M}\Omega\text{-cm}$ at 25 °C was used from a Milli-Q purification system (Merck KGaA, Darmstadt, Germany). Ethanol (>99%), 1-dodecene (>94%), dimethyloctadecyl[3-(trimethoxysilyl)propyl]ammonium chloride (60% in methanol), fluorescein sodium salt and polyethylenimine (PEI) were purchased from Sigma-Aldrich (Merck KGaA, Darmstadt, Germany). Octadecyltrimethoxysilane (97%) was purchased from ABCR (abcr GmbH, Karlsruhe, Germany) and ammonia (25% in water) was purchased from Acros Organics (Thermo Fisher Scientific, Geel, Belgium). The precursor (acetylacetonato)dicarbonylrhodium(I) (Rh-(acac)(CO)₂) was purchased from Umicore (Umicore AG & Co. KG, Hanau, Germany) and the water soluble ligand Sulfoxantphos was obtained by Molisa (Molisa GmbH, Magdeburg, Germany) where it was synthesized by the procedure of Goedheijt et al.³⁴. Argon 5.0 obtained from Linde (Linde GmbH, Pullach, Germany) was used for purging the sample and a syngas mixture of CO(purity 1.6):H₂ (purity 3.0) = 1:1 was used.

2.2 Synthesis of Silica Spheres and Modification

The silica particles were synthesized using the well-known sol-gel approach, called Stöber process³⁵. Different particle sizes were achieved by increasing the particle size of the core particles according to a protocol described by van Blaaderen³⁶. In this study, diameters of 50 nm and 100 nm were aimed as different particle sizes. The particle surface was modified by silanization using the

same silanes as Zhao et al.²² but with a different procedure and concentration. Negatively charged hydrophobic particles were obtained using octadecyltrimethoxysilane. The negative charge results from residual hydroxy groups at the silica surface³⁷. To obtain positively charged hydrophobic particles the same amount of dimethyloctadecyl[3-(trimethoxysilyl)propyl]ammonium chloride was used, which represents a silane with a similar hydrophobic chain length while simultaneously inducing a positive charge. For silanization, an amount of silane corresponding to roughly 2 silane molecules per nm² of particle surface was added. The reaction was then performed in ethanol at 20 °C with 200 rpm for 1 hour and an additional hour at 60 °C. After the reaction the solvent was completely removed by evaporation under vacuum and approximately 1.5 g white powder was obtained which was redispersed in a desired solvent by ultrasonication. The sample names describe the aimed particle diameters and the silane used for modification. Three different samples were prepared: smaller oppositely charged particles with an aimed diameter of 50 nm (50C18n+, 50C18n-) and larger positively charged particles with an aimed diameter of 100 nm (100C18n+). For the pristine particles the abbreviations 50pristine are used.

2.3 Preparation of Emulsion

The PEs were prepared using the IKA T25 Ultra-Turrax with a S25N-10G dispersing unit. First, the particles were dispersed by ultrasonication in the desired volume of oil for 10 min. Then, the water was added and the system was homogenized for 5 min at 20000 rpm. In case of the PEs containing the ligand Sulfoxantphos (SX) or the catalyst complex Rh-SX, the desired compound was first dissolved in the water phase in the vial. Different batch sizes were used for different purposes in order to use the limited amount of particles in one batch efficiently. A small batch with a total volume of 12.55 mL was used for emulsion characterization and a larger batch with a total volume of 39.58 mL was used for the reaction for simulating a more application-oriented approach³⁸. For the reaction, the water phase was fixed to 25 wt% with respect to the liquid phase (≈ 20 vol%) using 8 g water and 24 g 1-dodecene. While preparing the PEs for the catalysis additional steps were carried out to prevent the contact between the oxygen sensitive Rh-catalyst and air. First, the vessel used for the PE preparation was flushed with Ar, then the particle 1-dodecene suspension was added and the vessel was flushed again with Ar. The catalyst solution was introduced using a syringe and the emulsion process was started immediately under constant Ar stream above the vessel. After homogenization, the vessel was closed, shaken carefully and the emulsion was poured into the prepared and Ar flushed reactor.

2.4 Preparation of Catalyst Solution

For the hydroformylation catalyst, 38.5 mg (0.15 mmol, 1 eq.) of the precursor Rh(acac)(CO)₂ and 466.9 mg (0.6 mmol, 4 eq.) of the ligand SX were evacuated three times and flushed with Ar by using the Schlenk technique. 6 g of degassed water were added and the catalyst solution was stirred (700 rpm) for at least 12 h

at room temperature.

2.5 Instrumentation

2.5.1 a) Characterization of Particles

Pristine and modified particles were characterized by various techniques. The particle size was determined via image analysis of transmission electron microscopy (TEM) micrographs. The density of a single particle was determined by measuring the density of particle suspensions at different particle concentrations using a densitometer (DM40, Mettler Toledo). The hydrophobicity was quantified the contact angle measurements of a water droplet on a spin coated particle layer (OCA 15, DataPhysics). Atomic force microscopy (AFM) studies were carried out in order to ensure similar roughness of the particle layer. The charge of the particles was determined by ζ -potential measurements. Further information of the methods and the instrumentation are given in the supporting information.

2.5.2 b) Characterization of PEs

2.5.2.1 Fluorescence Microscopy The PE type (w/o or o/w) was identified by dyeing the water phase with the water soluble but oil insoluble fluoresceine sodium salt (uranine) at a concentration of $5.32 \cdot 10^{-3} \frac{\text{mmol}}{\text{L}}$. The images obtained were then coloured green using ImageJ for better readability.

2.5.2.2 Drop Size Distribution Determination The size of the water droplets was determined from micrographs taken from the PEs in less than 1 hour after preparation with Zeiss Imager A1 microscope and a 50x or a 20x objective, respectively. The PEs were shaken by hand and a droplet of a few microlitre was spread on a microscope slide. At least 15 images containing a total of 400 up to 800 different drops were recorded for every data point. The images were then analysed using an image analysis software (SOPAT GmbH, Germany) which provides the droplet size distributions and average mean droplet diameters.

2.5.2.3 Cryogenic Scanning Electron Microscopy (cryo-SEM)

The sample was secured into a cryo shuttle by use of a freezing rivet and submerged into slushed nitrogen. The sample was then transferred under vacuum into a Quorum PP3010 cryo preparation chamber which was under high vacuum and pre-cooled to -140 °C. The sample was fractured using a cooled knife. Prior to imaging, an Iridium coating was sputtered onto the samples and it was transferred into a Thermo scientific Helios G4 CX DualBeam (Focused ion beam scanning electron microscope; FIB-SEM) operating at 2 kV and 0.1 nA. The FIB-SEM is fitted with a cold stage (-140 °C) and cold finger (-175 °C).

2.5.2.4 Batch Reactor Test For the hydroformylation reaction in the batch reactor the PEs were prepared according to the description above. After PE preparation the emulsion was transferred into the batch reactor immediately. Syngas (1:1) with a pressure of 15 bar and a temperature of 100 °C was applied increasing both simultaneously from atmospheric pressure and room temperature. During heating and cooling the emulsion was stirred at 300 rpm while during the reaction over a duration of 20 hours the PE was stirred at 1200 rpm. The composition of the

product phase was determined by gas chromatography after the reaction.

2.5.2.5 Gas Chromatography (GC) A sample of 30 - 60 μL (1-2 drops) was taken from the batch at room temperature after the reaction. The sample was then diluted in isopropanol and the internal standard nonan was added. The composition of the sample was determined via the gas chromatography setup GC2010plus by Shimadzu from the height of the different maxima. For the measurement, the gas chromatography column Restek RTX5-MS (30 mm x 0.25 mm x 0.25 μm) was used.

2.5.3 c) Membrane Filtration

Filtration experiments were conducted at room temperature in a solvent resistant stirring cell (XFUF04701 by Merck KGaA, Darmstadt, Germany) with an active membrane area of 13.2 cm^2 .

An organic solvent nanofiltration membrane with a molecular weight cut-off (MWCO) of 900 Da was used (oNF-3, BOR-SIG Membrane Technology GmbH, Gladbeck, Germany). According to the manufacturers instructions, membrane samples were soaked in pure 1-dodecene for at least 2 hours prior to use for preconditioning. The membrane samples were then washed with pure 1-dodecene at a constant pressure of $p = 4$ bar for $t = 90$ min and the mass of permeate was recorded using a LabVIEW program. The flux was then calculated from the actual recorded permeate mass m , time t , solvent density ρ_s and active membrane area A_{eff} , according to eq. (1) and normalized with respect to the pure 1-dodecene flux from membrane pre-treatment:

$$J = \frac{\Delta m}{\rho_s A_{\text{eff}} \Delta t} \quad (1)$$

Applying 4 bars and stirring the emulsion at 500 rpm half of the continuous phase was extracted while recording the flux, i. e. the phase fraction increased from 25 wt% to 40 wt%.

3 Results

Particle Characterization

In this section, the particle properties (size, density, ζ -potential, and hydrophobicity) of the unmodified 50pristine and the modified 50C18n-, 50C18n+, and 100C18n+ silica particles are characterized. The experimentally obtained particle properties are summarized in Table 1.

The particle size was determined by TEM from a dried particle layer and at least 350 particles were analysed for each system. From the resulting diameter distribution the Sauter mean diameter was calculated. Figure 1 shows the TEM images of the nanospheres and their related size distribution histograms. The shape of the particles can be assumed as approximately spherical with the systems having Sauter mean diameters of around 50 nm and 100 nm, respectively.

The particles surface charge was estimated from ζ -potential measurements. The value of the ζ -potential of the positively and negatively charged modified silica particles is similar and about 50 mV having an opposite sign for surface charge (Table 1). The negative charge of the 50pristine and 50C18n- particles results from partially deprotonated OH groups at the surface³⁷.

Table 1 Summary of the experimental particle parameters: 50C18n- and 100C18n+ only differ in one property from the 50C18n+ sample. In case of 50C18n+ it is the sign of the ζ -potential and in case of 100C18n+ it is the specific cross section. d : Sauter mean diameter from TEM; ζ -potential measured in ethanol; ρ_p : total suspension density of the particle suspension; CA: contact angle of a water droplet on a particle layer; $a_{\theta,m}$: specific cross section; $4 \cdot a_{\theta,m}$: specific surface¹ 50pristine and 50C18n- density presumably similar to the density of 50C18n+. rms: root mean square roughness of particle layer

	50pristine	50C18n-	50C18n+	100C18n+
d / nm	46.3 ± 5	46.7 ± 5	45.7 ± 5	97.0 ± 5
CA / $^\circ$	24 ± 3	113 ± 3	107 ± 4	105 ± 3
ζ -potential / mV	-63 ± 3	-50 ± 3	$+53 \pm 4$	$+53 \pm 4$
$\rho_p / \frac{\text{g}}{\text{cm}^3}$	- ¹	- ¹	1.77 ± 0.04	1.93 ± 0.05
$a_{\theta,m} / \frac{\text{m}^2}{\text{g}}$	-	-	18.2 ± 0.4	8.0 ± 0.2
$4 \cdot a_{\theta,m} / \frac{\text{m}^2}{\text{g}}$	-	-	72.7 ± 1.5	32.0 ± 0.5
rms / nm	18 ± 3	13 ± 4	17 ± 4	29 ± 8

The hydrophobicity of the particles was determined from the wettability of a spin coated particle layer. All contact angles (CA) of a deposited water droplet on the prepared surfaces determined for the modified particles lay in the small interval between 105° and 113° (Table 1). The CA of the 50pristine layer lays around 24° , which is significantly lower than for the modified particles. The particle modification process successfully hydrophobized the particles (CA $> 90^\circ$) but did not turn them too hydrophobic (CA $< 120^\circ$). The results match very well with the observations for the particles dispersability behaviour: the hydrophobized particles are not dispersible in water (see Figure S1 particles floating on water) but form highly stable suspensions in ethanol. In addition to particle chemistry, the wettability of a surface depends strongly on its roughness³⁹. Therefore, the surface topography of the particle layers was studied by atomic force microscopy (AFM) (Figure S2). From the height distribution in Figure S2 the root mean square (rms) roughness was determined (Table 1). The rms is similar for all particle layers composed of the smaller modified and pristine particles (13-17 nm). The layer consisting of the larger particles exhibits a roughness approximately twice as high (29 ± 8 nm).

For determining the total particle cross section, knowledge of the particle density ρ_p is essential. For this, the total densities ρ_{tot} of particle suspensions with defined particle concentrations in ethanol were measured. The routine is explained in the supporting information (SI). Figure S3 shows the determined density reciprocal plotted over the particle concentration. In summary, the smaller particles exhibit a density of $(1.77 \pm 0.04) \frac{\text{g}}{\text{cm}^3}$ and the larger particle a slightly larger density of $(1.93 \pm 0.05) \frac{\text{g}}{\text{cm}^3}$. The total particle cross section per mass $a_{\theta,m}$ is calculated using eq. 2 (derivation in SI):

$$\frac{A_{\theta,\text{tot}}}{m_p} = a_{\theta,m} = \frac{3}{2\rho_p d_{3,2}} \quad (2)$$

In summary, it was found as expected, that the difference between 50C18n+ and 50C18n- lays in the sign of the ζ -potential while the difference between 50C18n+ and 100C18n+ is the specific

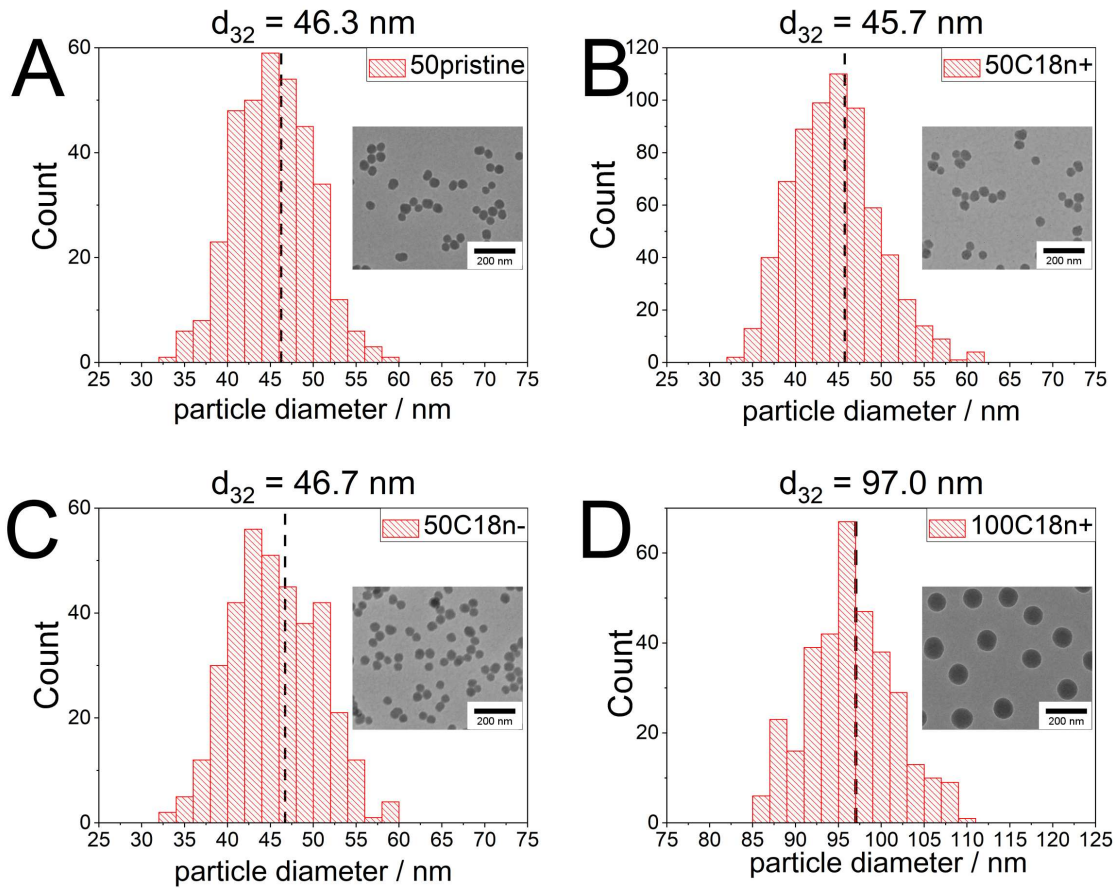


Figure 1 TEM-images of the pristine and the modified silica nanospheres. The Sauter mean diameter ($d_{3,2}$) was determined from the size distribution from image analysis.

cross section.

3.1 Emulsion Characterization

In the following, the ability of the particles to stabilize PEs is explored. Figure 2A shows photographs of emulsions with different particles 12 hours after preparation. The emulsion with untreated 50pristine particles is unstable and breaks within a few hours into the initial two phase system. The turbidity of the bottom phase (water) corresponds to the turbidity of the initial particle suspension and no emulsion droplets were identified under the microscope. The PEs stabilized by the modified particles sediment and form the white phase at the bottom of the flask. Studies by light microscopy after 12 hours (Figure 2B) show that the droplets stay intact. This stability was observed even after months and beyond. A fluorescein dyed version of each emulsion was investigated additionally by fluorescence microscopy, which confirms the water in oil type (w/o) of the PEs (Figure 2B).

The effect of water and particle fractions on the packing geometry of the 2D self assembly of the particles at the water/oil interface was studied for the positively charged particles by microscopy (Figure S4). The resulting Sauter mean droplet diameters (d_{PE}) are shown in Figure 3. d_{PE} of the droplets increases linearly with the water fraction. Measurements after approxi-

mately 2 months show that for the 40 mg 100C18n+ sample with 40 vol% water content the Sauter mean diameter increased from $72.4\mu\text{m}$ to $80.6\mu\text{m}$. For higher particle concentration or lower water content the differences were negligible. For water contents above 50 vol% double emulsions formed and the droplet diameter could not be determined (Figure S5).

The solid lines represent linear fits to the data. They are used to calculate the packing parameter s . The dashed lines result from a calculation assuming a hexagonal packing using eq. 3:

$$d_{PE} = \frac{6sV_{PE,tot}}{a_{0,m}m_{p,tot}} f_w = \frac{6sf_w V_{PE,tot}}{a_{0,m}m_{PE,tot}} \frac{1}{c_p} \quad (3)$$

Eq. 3 allows predicting PE droplet sizes when knowing the specific particle cross section $a_{0,m}$, the input particle weight $m_{p,tot}$, the total PE mass $m_{PE,tot}$, the total PE volume $V_{PE,tot}$, the used water fraction f_w and assuming a 2D hexagonal packing (packing parameter $s \approx 0.907$). The linear fits (solid lines) agree very well with these completely independent predictions.

The conformation of the particles at the water-oil-interface was studied by in-situ cryo-SEM of selected samples. The micrographs in Figure 4 show dense packing of the particles at the w/o interface. The micrographs reveal two kinds of structures on the droplet surface: a relief-like structure of missing particles in Fig-

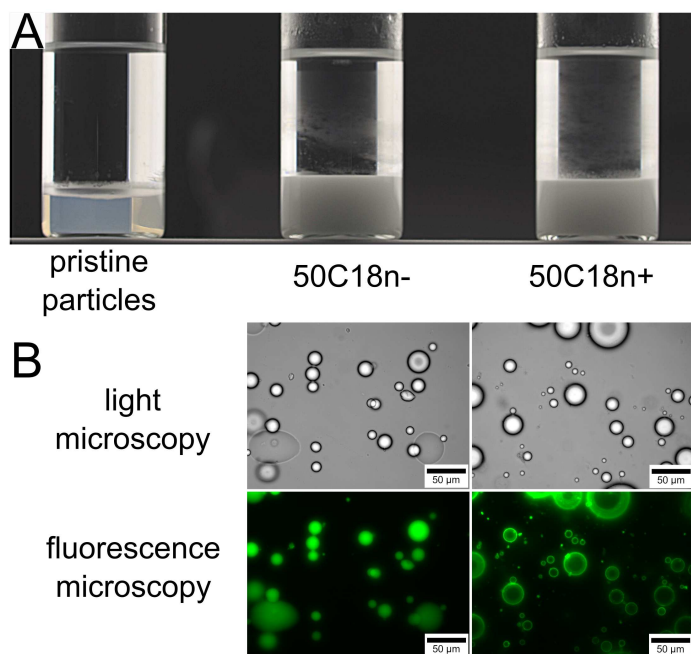


Figure 2 A: Photographs of water/dodecene PEs formed with three different particle (0.5 wt%) systems with a water fraction of 25 wt% (20 vol%) after 12 hours. While the hydrophobized particles are able to form stable PEs the pristine particles are not able to stabilize lasting emulsions. B: Related microscopy images for fluorescein dyed samples show intact droplets and fluorescence microscopy images proof the w/o type.

ure 4A and the particles occupying the interface in other regions in Figure 4B. The structure in panel A results most presumably from the sample preparation process in which the particles broke away during freezing and cutting. In both cases, a hexagonal like structure can be recognized.

3.2 Influence of Catalyst Particle Interaction

In this section, the influence of the catalyst on the emulsion structure is quantified. Stehl et al.²⁴ determined the surface tension of a ligand-water-solution (SX) against air and compared it to the catalyst-ligand-solution (RH-SX). The determined values for both substances are similar so that it was stated that the physical interfacial behaviour of the catalyst system is dominated by the ligand SX. Thus, for investigating the physical properties of the catalyst system it is sufficient to only use the cheaper SX instead of the expensive catalyst complex. In this work, the surface tension of an aqueous SX solution was measured against dodecene using the Du Noüy ring method (Figure 5). The curves follow a typical trend for a classical surfactant. In the interval between $10^{-4} \frac{\text{mol}}{\text{L}}$ and $10^{-2} \frac{\text{mol}}{\text{L}}$ the surface tension decreases by about $20 \frac{\text{mN}}{\text{m}}$ from slightly above $40 \frac{\text{mN}}{\text{m}}$ to slightly above $20 \frac{\text{mN}}{\text{m}}$. From this, the required space for one SX molecule was estimated to $a_{\text{SX}} = 0.96 \text{ nm}^2$ using the Gibbs equation⁴⁰.

The catalyst-particle interaction was quantified by the ζ -potential measurements in ethanol. The particles are not dispersible in water and the ligand is not soluble in oil. Although these measurements do not represent the reaction environment,

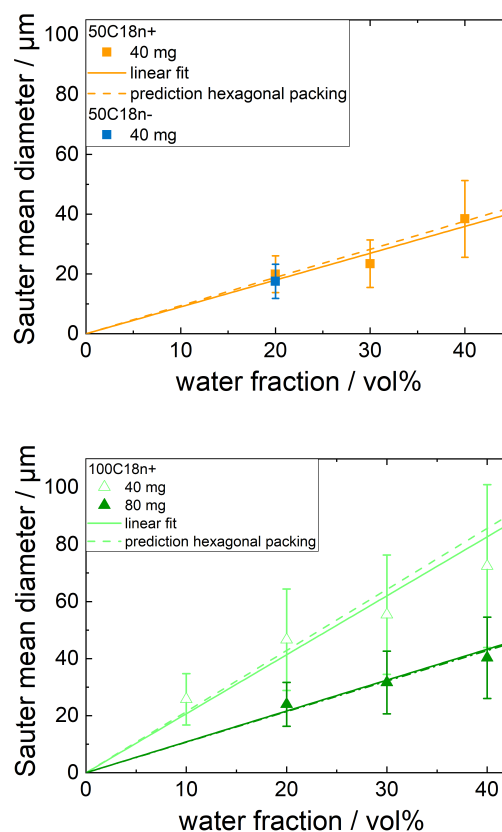


Figure 3 Sauter mean diameter d_{PE} for water/dodecene PEs at constant volume of 12.55 mL. Every point was calculated from 400 to 800 measured droplets. The error bars represent the standard deviation of each droplet size distribution. The Sauter mean diameter scales roughly linearly with the water fraction. The solid line represents a linear fit. The dashed lines were calculated using eq. 3 with the determined particle properties. The packing parameter was set to $s = 0.907$ assuming a hexagonal packing. The completely independent predictions agree well with the linear fits.

they reveal a general trend of the behavior of the ligands adsorption onto the particles. Figure 6 shows the measured ζ -potential for the particle-SX-complexes as a function of the ligand amount per particle area k_n . The concentration of SX was normalized with respect to the total surface of the added particles, which was calculated from particle size (TEM) and density data (Table 1). The potentials of both initially positively charged particles 100C18n+ and 50C18n+ show a decrease with increasing k_n , i. e. SX, and even change sign at about 2-6 molecules per nm^2 . The curves of both positively charged particles nearly overlay each other. The potentials of the negatively charged particles do not change with the catalyst concentration.

Both, the surface activity of the ligand SX and its ability to adsorb onto the positively charged particles are presumed to affect the PEs structure. For further investigations, PEs were prepared with and without SX to compare the droplet sizes. Different PEs with a constant water fraction of 20 vol%, a constant total volume and a constant amount of SX were produced (Figure S6). The particle concentrations were varied and their droplet size dis-

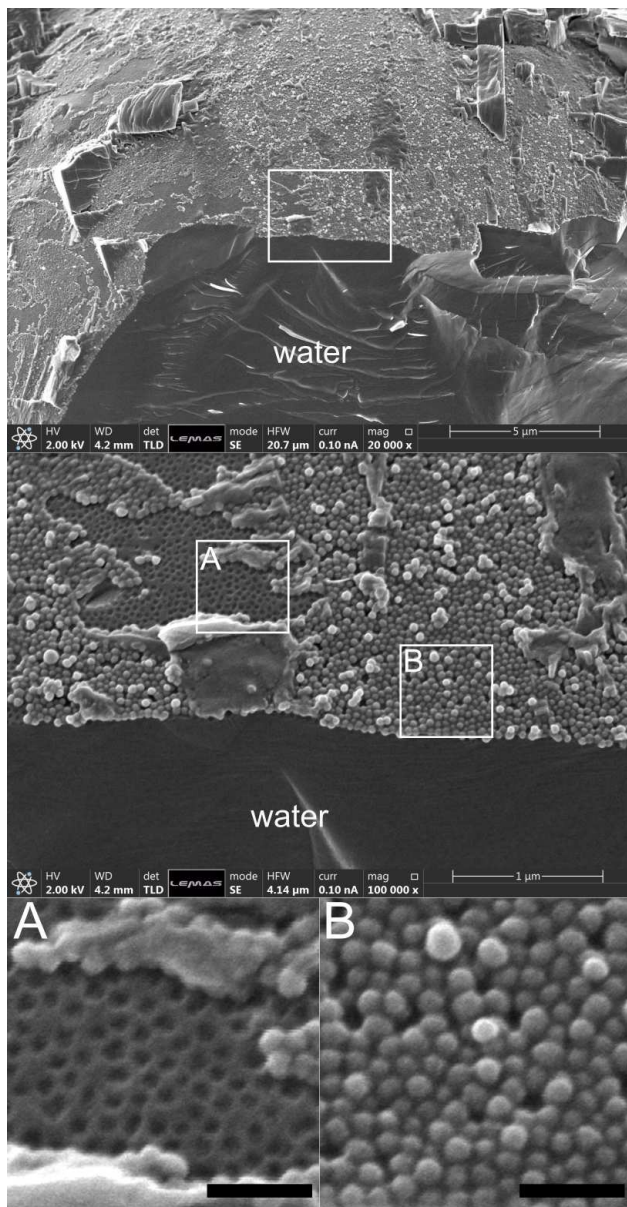


Figure 4 Cryo-SEM images of water/dodecene PEs with particle concentration $c_p = 0.5\text{ wt}\%$ and water fraction 20 vol% using 50C18n+ particles. The particles form a structure similar to the 2D hexagonal close packing. This is well recognizable in the areas where the particles broke away in the preparation process and left gaps behind (A). The length of the black bars in (A) and (B) corresponds to 200 nm. The images were taken about one week after emulsification.

tributions were determined. The results for the measured Sauter mean diameters are shown in Figure 7. In both cases (with and without SX), the curves follow a trend reciprocal to the added particle mass as predicted by eq. 3. The predicted values calculated from experimental particle properties (Table 1) are shown as a dashed line. The calculated values are in perfect agreement with the $d_{PE} = \frac{\text{const.}}{c_p}$ fit. The addition of SX leads to a reduction of the droplet size and by fitting eq. (3) a decrease of the packing parameter from $s = 0.92 \pm 0.05$ to $s = 0.69 \pm 0.01$ was determined. The effect of SX reducing the droplet size was seen irrespectively of size and charge (Figure S7).

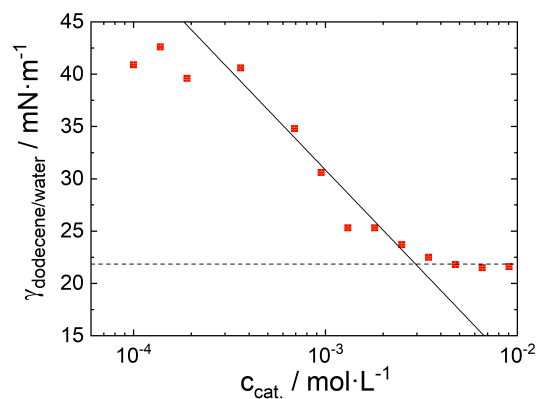


Figure 5 Measured surface tension γ for a SX solution in water at the water/oil interface using Du Noüy ring method. γ decreases with increasing SX concentration until it reaches a plateau (dashed line) at $3 \cdot 10^{-3} \text{ mol/L}$. To get a value for the occupied space of a single SX molecule the Gibbs equation was fit to the data (solid line). The required space for a single molecule was estimated to $a_{SX} = 0.96 \text{ nm}^2$. During the reaction, the concentration of the ligand in the water phase of the PE is $\approx 0.075 \text{ mol/L}$.

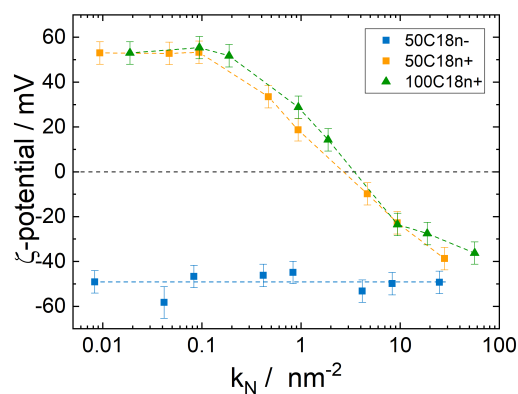


Figure 6 ζ -potential as a function of the concentration of SX per particle area (k_n). The ligand SX decreases the ζ -potential for both positively charged particle types while the ζ -potential of the negatively charged particles is not influenced by the presence of SX.

These findings raise the question whether the presence of catalyst modifies the particle ordering at the droplet surface. For answering this, cryo-SEM images were recorded of PEs containing SX one week after preparation (Figure 8). Comparing these new images for PEs containing SX with the images of PEs without SX (Figure 4) a more shattered surface occupation structure of the particles is observed for both particle systems 50C18n+ and 50C18n-. Voids can be found between the particles in the form of smooth areas in the particle formed relief in (A) and (C) as well as in the visible particle layer in (B) and (D) between the particles.

3.3 Hydroformylation of 1-Dodecene

In the next step, the hydroformylation of 1-dodecene was studied in PE environment in a batch reactor. The PEs total volume was increased by a factor of approximately 4 to 24 g oil and 8 g aque-

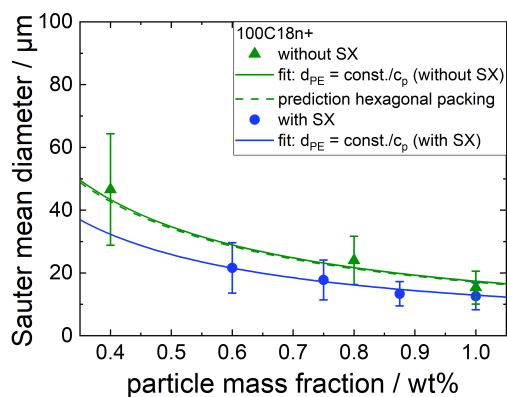


Figure 7 Sauter mean diameters for PEs produced with different 100C18n+ particle concentrations with SX ($0.015 \frac{\text{mol}}{\text{L}} \approx 147 \text{ mg}$) and without SX for a water fraction of 20 vol% and 1-dodecene as continuous phase. The error bars represent the standard deviation of each droplet size distribution. The dashed line was calculated using eq. 3 with the determined particle properties above and setting $s = 0.907$. The straight lines represent a non linear fit with the form $d_{PE} = \frac{\text{const.}}{c_p}$ (according to eq.(3)). The packing parameters were calculated from the fits to $s = 0.92 \pm 0.05$ (without SX) and $s = 0.69 \pm 0.01$ (with SX).

ous catalyst solution. Compared to the 50C18n+/- system twice the mass fraction of 100C18n+ particles was used to achieve a similar droplet diameter in the reactive system. This minimizes the influence of the droplet size and curvature on the reaction yield. The space time yield is shown in Figure 9A. Other related reaction results are summarized in Table 2.

Table 2 Reaction related parameters. * calculated with eq. (4) using $s = 0.69$ ** calculated with eq. (5)

	50C18n- (0.5 wt%)	50C18n+ (0.5 wt%)	100C18n+ (1 wt%)
conversion / %	1.4	7.6	6.3
selectivity / %	64	78	87
TON	13.7	72.4	60.4
conv. rate per total void area $/ \frac{1}{\text{nm}^2\text{h}}$ *	46.3	-	-
conv. rate per total oil contact area $/ \frac{1}{\text{nm}^2\text{h}}$ **	-	45.7	43.1

The space time yield for positively charged particles is significantly higher than for negatively charged ones. Moreover, it was found that the particle size has no impact on the space time yield when the difference in particle size is compensated by the mass fraction. Nevertheless, the PEs containing the particles were identified to be less stable. After the reaction, a thin layer of excess water ($\approx 5 \text{ vol\%}$) was found denoting that at least some of the droplets broke during the reaction. This was not the case for the PEs stabilized with the 50C18n+/- spheres. When knowing the packing parameter in a catalyst containing system to change from $s \approx 0.91$ to $s = 0.69$ (Figure 7) the conversion rate per active

(CRAA) area can be calculated. From the ζ -potential measurements in the presence of SX, it was assumed that for the negatively charged particles the reaction exclusively takes place in the voids between the particles at the oil /water interface. Therefore, the conversion in number of molecules achieved was divided by the total void area. The total void area can be calculated using eq. 4:

$$A_{\text{void,tot}} = (1 - s)A_{PE,\text{tot}} = A_{\theta,\text{tot}} \frac{1 - s}{s} \quad (4)$$

with $A_{\theta,\text{tot}} = sA_{W/O,\text{tot}}$ ($A_{PE,\text{tot}}$: total droplet surface area), which is only dependent on the packing parameter s and the input total particle cross section $A_{\theta,\text{tot}}$. In case of the positively charged 50C18n+ and 100C18n+ particles, the reaction takes place at both the w/o interface and the particle surface. Therefore, the achieved conversion per active area requires the inclusion of the particle surface protruding into the oil phase. This total active area includes the particle-oil contact area and the total void area and is calculated by eq. 5:

$$A_{\text{oil contact}} = \frac{1}{2} \cdot 4 \cdot A_{\theta,\text{tot}} + A_{\text{void,tot}} = A_{\theta,\text{tot}} \frac{1 + s}{s} \quad (5)$$

The difference between the total void area and the total substrate contact area are illustrated schematically in Figure 10. The determined values for the conversion per active surface are very similar for all three samples around $45 \frac{1}{\text{nm}^2\text{h}}$ with only a difference of about 7% (Figure 9B or Table 2).

3.4 Membrane filtration

In this section, the potential of catalyst recovery via membrane filtration of the PEs after reaction is elaborated. For this, the PEs are transferred into the corresponding equipment. Under constant stirring and applied pressure of 4 bars, the organic phase (consisting of 1-dodecene and the products from the hydroformylation reaction) was filtered through the membrane while the particle-stabilized dispersed phase droplets containing the valuable catalyst were retained by the organic solvent nanofiltration membrane. A stable flux was reached after only a few minutes and stayed constant until the filtration was stopped after 50 wt% of the organic phase had permeated. Figure 11A shows the measured flux normalized with respect to the flux of pure 1-dodecene from the membrane pretreatment. A stable flux was reached after only a few minutes and stayed constant until the filtration was stopped. The particles surface charge seem to play a minor role if any at all. The normalized flux curves are similar to each other with no significant deviation. The slight deviation for 50C18n+ may be explained by small inherent differences in different membranes used. The droplet size was measured for a freshly prepared emulsion, after the reaction and after filtration of 50 wt% of the product phase with a microscope (Figure 11B and Figure S6). The results show that the Sauter mean diameter is preserved after each filtration step. This stability of the PEs enables continuous reaction processes with droplet recycling via membrane filtration. Again, the charge and size are found to have no influence on the Sauter mean diameters of the recycled emulsion droplets.

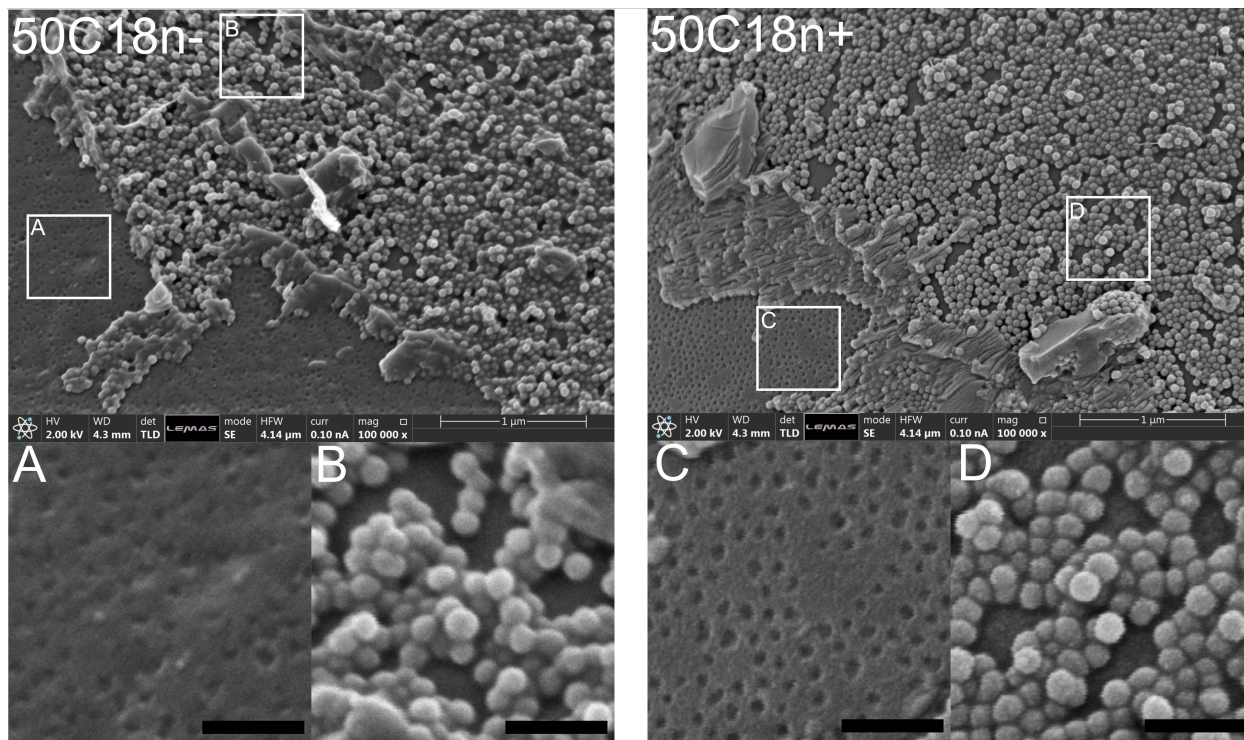


Figure 8 Cryo-SEM images of PEs produced with 50C18n- (left) and 50C18n+ (right) (water fraction 20 vol%, particle mass fraction 0.5wt%) in presence of SX ($0.015 \frac{\text{mol}}{\text{L}}$). In both cases the addition of SX results in numerous voids in the structure. This effect can be seen in the areas where particle broke away and the relief was scanned (A) and (C) as well as in the particle structure present on the droplets surface (B) and (D). SX has molecular size and is invisible in the SEM picture. The images were taken roughly one week after emulsification. The black bars in (A) - (D) represent 200 nm.

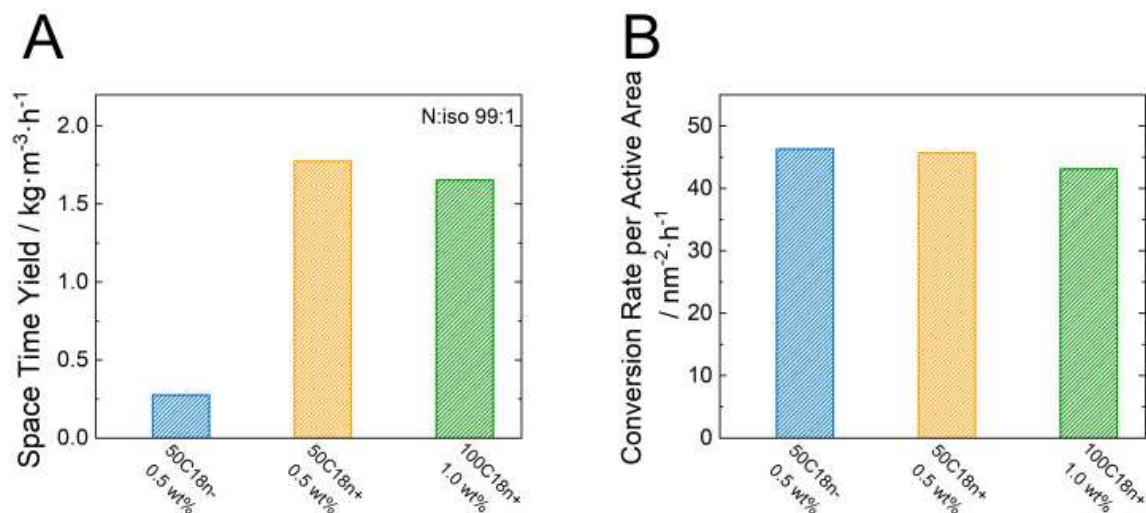


Figure 9 (A) Reaction results for the space time yield using a larger batch with 32 g in total for the whole PE. Reaction conditions: catalyst:ligand = 1:4, amount of catalyst: $146 \cdot 10^{-3} \text{ mmol}$, S/C = 960, amount of particle 160 mg 50C18n+/- and 320 mg 100C18n+, water fraction 20 vol% (B) Conversion rate per active area (CRAA) calculated using eq. 4 for PEs with 50C18n- and eq. 5 for PEs with 50C18n+ and 100C18n+.

4 Discussion

4.1 Structure of PEs

Modified and comparable silica particles varying in size (50 & 100 nm in diameter) and charge (+/-) were successfully produced and characterized in terms of their particle parameters. The

characterised parameters are particle charge, size, shape, density, and specific particle cross section. The samples 50C18n- and 50C18n+ have very similar size but an opposing surface charge. The samples 50C18n+ and 100C18n+ have quite the same surface charge but vary significantly in size.

The particles were used to produce very stable PEs of w/o type.

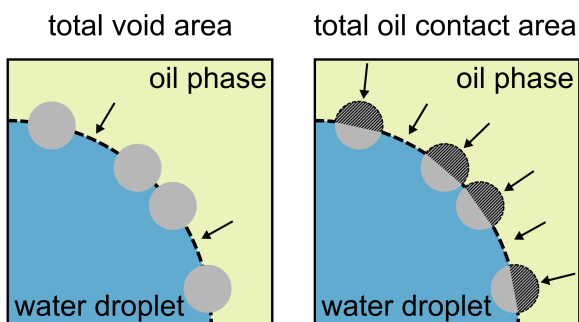


Figure 10 Illustration of the two different types of catalytic active interface. The total void area (left) includes only the water/oil interfacial area, which is the only active area for the negatively charged particles. The total substrate contact area (right) includes the voids as well as the particle surface area protruding into the oil phase. This is the active area for the positively charged particles because the catalyst is also able to adsorb on the particle surface.

The droplet size in dependence of the water fraction was shown to follow eq. 3 proving that the droplet size can be easily predicted by the given total emulsion volume and the determined particle cross section under the assumption of a hexagonal packing. The other way around, the particle density at the droplet interface can be determined for known droplet sizes. The validity of the model assumptions is proven by the very good agreement of the predictions and the experimental data points. The first assumption states that nearly all particles adsorb at the droplet interface. The second stating hexagonal packing of the particles at the w/o interface is the most probable ordering at the droplet surface. These are important observations because insights into the surface ordering of the particles in a Pickering emulsion system are generally difficult to resolve experimentally: light microscopy methods are limited to the regime beyond the micrometer scale. Scattering and reflectometry techniques heavily rely on complex models with many parameters and their interpretation becomes vague when dealing with multiple interfaces at once. Even rare and elaborate imaging methods like cryo-SEM only show the frozen state and neglect the dynamics of the system in-situ. Anyhow, cryo-SEM is up to now by far the best approach to investigate the ordering of nm-sized solid particles at liquid interfaces⁴¹. The images obtained by cryo-SEM for selected emulsions confirm the results above. In these images (Figure 4), a very dense particle monolayer corresponding to a hexagonal packing is observed. The surface charge of the particles seems not to be strong enough to separate the particles so that the free space between the particles is limited to the very small voids caused by hexagonal packing. It shows that with a simple model and the knowledge of the necessary parameters a good estimation of the droplet diameter is valid.

In the following, the influence of the catalyst on the emulsion structure is discussed. The space for one SX molecule at the water/dodecene interface was estimated to $a_{SX} = 0.96 \text{ nm}^2$ using Gibbs law. This corresponds to a density of roughly one molecule per nm^2 present at the water/dodecene interface. By using a cat-

alyst to ligand ratio of 1:4 means that in the reaction in average one active molecule of catalyst is found every 4 nm^2 in the void area. While the catalyst is adsorbed to the interface minimizing its free energy, it is attracted by the particles positive surface charge electrostatically. The ζ -potential measurements confirm the strong attraction between the negatively charged SX molecules and the positively charged particles but not with the negatively charged ones. The charge reversal of the particle-SX-complex with increasing SX concentration is explained by adsorption of SX onto the particle surface. This adsorption is solely dependent on the total particle surface: the curves for 50C18n+ and 100C18n+ show strong coincidence after normalizing the SX concentration with respect to the total particle surface. Since the diameter of several 10's of nm is much larger than the molecular size of a catalyst the curvature seems to have no impact here.

The surface activity of SX was found to modify the structure of the PEs by introducing large voids into the packing of the particles (Figure 4) leading to a shattered internal structure (Figure 8 and Figure 12A). This explains the smaller droplet sizes found for PEs prepared with SX. Additionally, this is why the droplet diameter cannot be predicted by eq. 3 which assumes a hexagonal packing of the particles at the droplet surface. Interestingly, the droplet size values for PEs with SX remain proportional to the reciprocal particle concentration (Figure 7).

4.2 Hydroformylation of 1-Dodecene

The interaction between the catalyst and the particles has a prominent impact on the reaction performance. In all investigated PEs the dense particle layer at the o/w interface hinders the mass transport to the catalyst, explaining the overall slow reaction rates. Nevertheless, the data allow some important conclusions. While the particle charge has no pronounced impact on the PE structure, a difference in yield was measured for the oppositely charged particles 50C18n+ and 50C18n- (Figure 9A). The yield for 50C18n+ is up to 550% higher than for 50C18n- even though the determined droplet size for all PEs was very similar during the whole process (Figure 11B). The only measured difference between both systems is the ability of 50C18n+ to attract and immobilize the catalyst molecules. The immobilization of the catalyst on the particles surface enhances thus the reaction yield for the positively charged particles (Figure 12A and Table 2).

In summary, in case of 50C18n+ and 100C18n+ the particle oil interface is catalytically active which is not the case for 50C18n-. At this point, only the deep knowledge of the interfacial adsorption behaviour of the SX molecules, the packing parameter and the PEs stability during the process enables more detailed insights, as demonstrated in the following.

The calculation of the conversion rates per active area is only possible when s and $A_{0,tot}$ are known, the PE is stable and nearly all particles are located at the interface. In this way calculated conversion rates are normalized with respect to the total area of individual active interface (taking the convex particle oil interface into account for 50C18n+ and 100C18n+) and are very similar to each other (Figure 9B). This leads to the conclusion that any interface where the catalyst is present is equally contributing to the

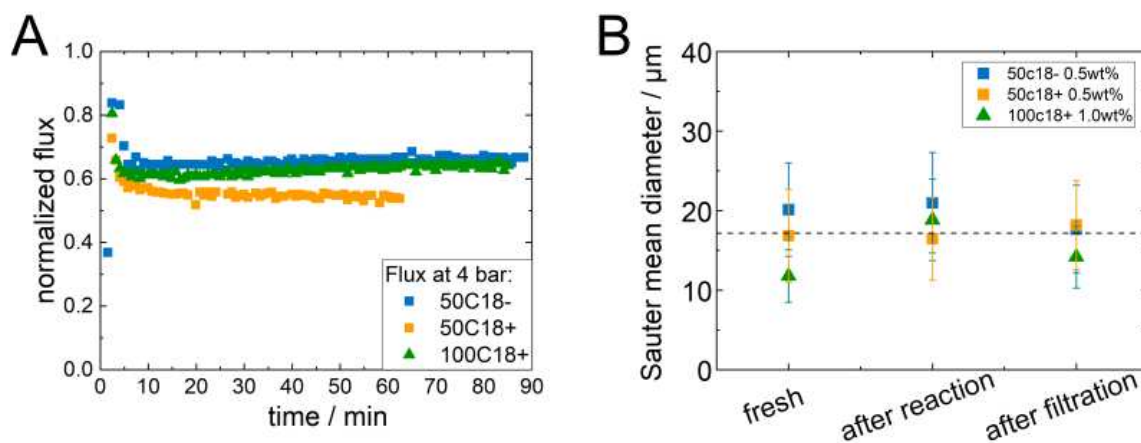


Figure 11 (A) Flux during the separation of the product phase via membrane filtration. (B) Droplet size before and after the reaction as well as after the filtration. It was proven that the PEs stayed intact over the whole process and the droplet size did not change.

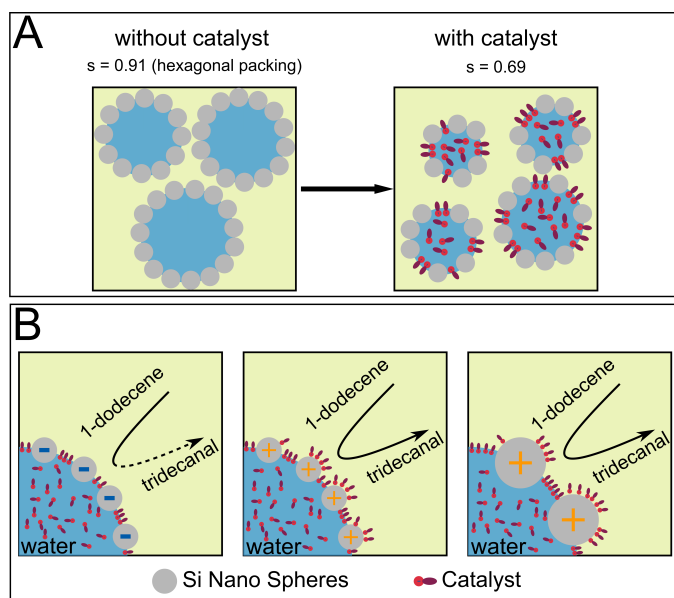


Figure 12 Illustration of the proposed model. (A) The catalyst molecules are able to decrease the packing parameter of the particles at the droplet interface. (B) The negatively charged and surfactant-like catalyst molecules adsorb onto the positively charged particles but not on the negatively charged ones. This results in a strong increase in reaction yield for the systems containing positively charged particles. Catalyst molecules on the particle surface seem to dominate the reaction process in the present system but the reaction takes place similar effective in both areas the voids and the particle surface.

total conversion. The other way around, this also implies that the SX concentration at the particle oil interface and in the void area between the particles is similar (≈ 1 per nm^2). The SX to particle surface ratio in the reaction was 43 molecules per nm^2 . If only the particle area in contact with the substrate phase is taken into account, the value corresponds to 86 molecules per nm^2 . Subtracting the amount of catalyst at the o/w interface still leads to the assumption that most of the catalyst molecules rather remain in the "bulk" of the droplets than participating in the reaction.

A turn over frequency (TOF_{int}) for only the catalyst molecules at the active interface is calculated using eq 6:

$$\text{TOF}_{\text{int}} = \text{CRAA} \cdot a_{\text{SX}} \cdot f_{\text{l:c}} \quad (6)$$

$f_{\text{l:c}}$ is the ligand to catalyst fraction. The resulting value of around $\text{TOF}_{\text{int}} \approx 180 \text{ h}^{-1}$ is considered as highly speculative but is also the only number independent from the PE structure describing the efficiency of the catalyst. For future formulations the used amount of catalyst needs to be adjusted to its adsorption properties towards the interface (particle surface and void interface). Here, 1 SX molecule per nm^2 is the ideal case, corresponding to the area per molecule of the catalyst. However, in reality this is hardly possible because of equilibration of SX molecules in the bulk and adsorbed at the interface.

Even though the internal sizing parameters differ, the reaction yield from the PEs stabilized by 50C18n+ and 100C18n+ (only 7% lower for 100C18n+) is similar as shown in Figure 9B. In the particle rich areas at the patchy droplet interface the single void size between the 100C18n+ particles in a 2D hexagonal layer is approximately 380 nm^2 while for 50C18n+ it is only 84 nm^2 . This means, that the size of single voids between the particles does not play a dominant role. Furthermore, the dynamics of the flux of substrate towards the voids is not a determining factor either.

4.3 Membrane Filtration

Regarding the results for the filtration process, the dense particle layer at the w/o seems very beneficial for the droplet and catalyst retention. After a few minutes a constant flux is achieved and the PEs droplet size did not change significantly during the filtration process. At least 50% of the oil phase could be removed without difficulties and a clear permeate with no water breakthrough was obtained. The minimal necessary amount of oil phase before breakup was not determined. Neither the particle surface charge nor the particle size has a significant influence on the

filtration performance. The experience obtained shows, that using membrane filtration for droplet and catalyst retention in PEs is very reliable and therefore very promising.

5 Conclusion

The study presents a detailed physico-chemical analysis of w/o Pickering Emulsions from the nanosized particle level to the micrometer-sized domains of the emulsion structure. Special attention was drawn to the surface-active catalysts influence on the PE structure and its location during the reaction process. Particles with almost identical hydrophobicity, shape and value of the zeta potential but with targeted opposite charges or difference in size respectively were successfully synthesized. This approach allowed studying the effect of one separated particle feature while other influencing factors could be excluded. Reliable quantitative prediction of the droplet size in PEs is possible using a simple model which requires basic information about the particle properties such as size and density. The predictions for the droplet diameter agreed even quantitatively perfectly with the independently measured droplet diameters proving the validity of all assumptions made. The packing parameter for the investigated system corresponds to a hexagonal 2D lattice. Neither the size nor the charge of the particles had an influence on the packing parameter. The packing parameter was reduced (from $s = 0.91$ to $s = 0.69$) after adding the catalyst to the PE. This did not diminish the PE stability. This stability was proven and utilized when using the PEs as a reaction environment and the subsequent performance of a membrane filtration for product separation. The particle surface charge has a strong effect on the reaction yield while the particle size itself is not a determining factor. Obviously, the adsorption of the (negatively charged) catalyst onto the (positively charged) particles favours the reaction. In addition to previous studies, it could be shown that this increase in conversion is even quantitatively explained by the geometry of the system. In case of a positive surface charge of the particles the particle-oil interface acts as an additional active surface and therefore the yield is increased. The other way around it was shown that the catalytic efficiency of both the water-oil and the particle-oil interface is roughly equal with a conversion of around 45 molecules per nm^2 and hour. This indicates that the amount of catalyst molecules at the oil-water interface is equal to the adsorbed catalyst molecules at the particles surface. The amount of ligand at the w/o interface was determined to be roughly 1 molecule per nm^2 . So all in all the reaction takes place at the surface of the particles as well as in the void between the particles. For future PE designs the active interface can be effectively increased in both ways, increasing the voids or increasing the particle surface indenting into the oil phase. But still the most important requirement should stay the verification of a sufficient PE stability. The successful membrane filtration (using oNF-3 membranes) of the oil phase from the water droplet phase without damaging the emulsion proved this sufficient stability for the present system and demonstrates the possible application of a continuously driven catalytic process.

6 Acknowledgments

Gefördert durch die Deutsche Forschungsgemeinschaft (DFG) - TRR 63 "Integrierte chemische Prozesse in flüssigen Mehrphasensystemen" (Teilprojekte B6, A10) - 56091768.

Funded by the Deutsche Forschungsgemeinschaft (DFG, German Research Foundation) - TRR 63 "Integrated Chemical Processes in Liquid Multiphase Systems" (subprojects B6, A10) - 56091768.

Additionally funded by Engineering and Physical Sciences Research Council (EPSRC), UK under grant EP/P00122X/1 and EP/R043388/1.

MG and AS acknowledge the German Research Foundation in the frame of the project GA-2169/5-1 for partial financial support of this work.

References

- 1 S. U. Pickering, *J. Chem. Soc., Trans.*, 1907, **91**, 2001–2021.
- 2 W. Ramsden, *Royal Society*, **31 January 1904**, 477–486.
- 3 C. L. Harman, M. A. Patel, S. Guldin and G.-L. Davies, *Current Opinion in Colloid & Interface Science*, 2019, **39**, 173–189.
- 4 J. Marto, A. Ascenso, S. Simoes, A. J. Almeida and H. M. Ribeiro, *Expert opinion on drug delivery*, 2016, **13**, 1093–1107.
- 5 B. S. Murray, *Current Opinion in Food Science*, 2019, **27**, 57–63.
- 6 L. Ye, T. Zhou and X. Shen, *Molecular Imprinting*, 2015, **3**, 257.
- 7 S. Wiese, A. C. Spiess and W. Richtering, *Angewandte Chemie (International ed. in English)*, 2013, **52**, 576–579.
- 8 A. Heyse, C. Plikat, M. Grün, S. Delaval, M. Ansorge-Schumacher and A. Drews, *Process Biochemistry*, 2018, **72**, 86–95.
- 9 S. Yu, D. Zhang, J. Jiang, Z. Cui, W. Xia, B. P. Binks and H. Yang, *Green Chemistry*, 2019, **136**, 7498.
- 10 L. Fu, S. Li, Z. Han, H. Liu and H. Yang, *Chemical communications (Cambridge, England)*, 2014, **50**, 10045–10048.
- 11 H. Yang, X. Rong and D. Wang, in *Encyclopedia of Polymeric Nanomaterials*, ed. S. Kobayashi and K. Müllen, Springer Berlin Heidelberg, Berlin, Heidelberg, 2014, vol. 109, pp. 1–17.
- 12 G. Lv, F. Wang, X. Zhang and B. P. Binks, *Langmuir*, 2018, **34**, 302–310.
- 13 L. Leclercq, A. Mouret, A. Proust, V. Schmitt, P. Bauduin, J.-M. Aubry and V. Nardello-Rataj, *Chemistry (Weinheim an der Bergstrasse, Germany)*, 2012, **18**, 14352–14358.
- 14 W.-J. Zhou, L. Fang, Z. Fan, B. Albela, L. Bonneviot, F. de Campo, M. Pera-Titus and J.-M. Clacens, *Journal of the American Chemical Society*, 2014, **136**, 4869–4872.
- 15 K. Hiebler, G. J. Lichtenegger, M. C. Maier, E. S. Park, R. Gonzales-Groom, B. P. Binks and H. Gruber-Woelfler, *Beilstein journal of organic chemistry*, 2018, **14**, 648–658.
- 16 X. Yang, Y. Liang, Y. Cheng, W. Song, X. Wang, Z. Wang and J. Qiu, *Catalysis Communications*, 2014, **47**, 28–31.
- 17 J. Cho, J. Cho, H. Kim, M. Lim, H. Jo, H. Kim, S.-J. Min, H. Rhee and J. W. Kim, *Green Chemistry*, 2018, **20**, 2840–

- 2844.
- 18 Y. Li, G. Zhao, B. Hong, S. Zhao, X. Han and M. Pera-Titus, *Colloids and Surfaces A: Physicochemical and Engineering Aspects*, 2020, **599**, 124800.
 - 19 R. von Klitzing, D. Stehl, T. Pogrzeba, R. Schomäcker, R. Minullina, A. Panchal, S. Konnova, R. Fakhrollin, J. Koetz, H. Möhwald and Y. Lvov, *Advanced Materials Interfaces*, 2017, **4**, 1600435.
 - 20 T. Skale, D. Stehl, L. Hohl, M. Kraume, R. von Klitzing and A. Drews, *Chemie Ingenieur Technik*, 2016, **88**, 1827–1832.
 - 21 D. Stehl, L. Hohl, M. Schmidt, J. Hübner, M. Lehmann, M. Kraume, R. Schomäcker and R. von Klitzing, *Chemie Ingenieur Technik*, 2016, **88**, 1806–1814.
 - 22 Y. Zhao, X. Zhang, J. Sanjeevi and Q. Yang, *Journal of Catalysis*, 2016, **334**, 52–59.
 - 23 L. Tao, M. Zhong, J. Chen, S. Jayakumar, L. Liu, H. Li and Q. Yang, *Green Chemistry*, 2018, **20**, 188–196.
 - 24 D. Stehl, N. Milojević, S. Stock, R. Schomäcker and R. von Klitzing, *Industrial & Engineering Chemistry Research*, 2019, **58**, 2524–2536.
 - 25 B. P. Binks and S. O. Lumsdon, *Langmuir*, 2001, **17**, 4540–4547.
 - 26 B. P. Binks and S. O. Lumsdon, *Langmuir*, 2000, **16**, 8622–8631.
 - 27 B. P. Binks, *Current Opinion in Colloid & Interface Science*, 2002, **7**, 21–41.
 - 28 O. Owoseni, Y. Zhang, Y. Su, J. He, G. L. McPherson, A. Bose and V. T. John, *Langmuir*, 2015, **31**, 13700–13707.
 - 29 R. Wiley, *Journal of Colloid Science*, 1954, **9**, 427–437.
 - 30 T. H. Whitesides and D. S. Ross, *Journal of colloid and interface science*, 1995, **169**, 48–59.
 - 31 M. Destribats, M. Eyharts, V. Lapeyre, E. Sellier, I. Varga, V. Ravaine and V. Schmitt, *Langmuir*, 2014, **30**, 1768–1777.
 - 32 T. Nallamilli, E. Mani and M. G. Basavaraj, *Langmuir*, 2014, **30**, 9336–9345.
 - 33 S. Arditty, C. P. Whitby, B. P. Binks, V. Schmitt and F. Leal-Calderon, *The European physical journal. E, Soft matter*, 2003, **11**, 273–281.
 - 34 M. Schreuder Goedheijt, P. C. Kamer and P. W. van Leeuwen, *Journal of Molecular Catalysis A: Chemical*, 1998, **134**, 243–249.
 - 35 W. Stöber, A. Fink and E. Bohn, *Journal of colloid and interface science*, 1968, **26**, 62–69.
 - 36 C. Graf and A. van Blaaderen, *Langmuir*, 2002, **18**, 524–534.
 - 37 M. Barisik, S. Atalay, A. Beskok and S. Qian, *The Journal of Physical Chemistry C*, 2014, **118**, 1836–1842.
 - 38 M. Vivien Kempin, M. Kraume and A. Drews, *Journal of colloid and interface science*, 2020.
 - 39 R. N. Wenzel, *Industrial & Engineering Chemistry Research*, 1936, 988–994.
 - 40 D. W. Gruen and J. Wolfe, *Biochimica et Biophysica Acta (BBA) - Biomembranes*, 1982, **688**, 572–580.
 - 41 L. E. Low, S. P. Siva, Y. K. Ho, E. S. Chan and B. T. Tey, *Advances in colloid and interface science*, 2020, **277**, 102117.